Journal of Manufacturing Processes 97 (2023) 100–114

Contents lists available at ScienceDirect

Journal of Manufacturing Processes

journal homepage: www.elsevier.com/locate/manpro

Production of the cylinder head and crankcase of a small internal combustion engine using metal laser powder bed fusion

Jamee Gray [a], Christopher Depcik [a,*], Jennifer M. Sietins [b], Andelle Kudzal [c], Ryan Rogers [b], Kyu Cho [b]

[a] University of Kansas, Department of Mechanical Engineering, Lawrence, KS 66045, USA
[b] Army Research Laboratory, Aberdeen Proving Ground, MD 21005, USA
[c] Naval Surface Warfare Center Carderock, Bethesda, MD 20817, USA

ARTICLE INFO

Keywords:
Internal combustion engines
Metal laser powder bed fusion
Computed tomography
Additive manufacturing
Porosity analysis
Reverse engineering

ABSTRACT

This effort investigates the use of metal additive manufacturing, specifically laser powder bed fusion (LPBF) for the automotive and defense industries by demonstrating its feasibility to produce working internal combustion (IC) engine components. Through reverse engineering, model modifications, parameter selection, build layout optimization, and support structure design, the production of a titanium crankcase and aluminum cylinder head for a small IC engine was made possible. Computed tomography (CT) scans were subsequently used to quantify whether defects such as cracks, geometric deviations, and porosity were present or critical. Once viability of the parts was established, machining and other post-possessing were completed to create functional parts. Final X-ray CT and micro-CT results showed all critical features fell within ±0.127 mm of the original equipment manufacturer (OEM) parts. This allowed reassembly of the engine without any issues hindering later successful operation. Furthermore, the LPBF parts had significantly reduced porosity percentages, potentially making them more robust than their cast counterparts.

1. Introduction

Additive manufacturing (AM) has numerous potential benefits, especially when considering the production of an internal combustion (IC) engine [1]. Since AM does not have the same constraints that limit traditional methods, such as casting or Computer Numerical Controlling, when used in conjunction with topology optimization, it allows for the design of structurally efficient lightweight designs capable of the same strength and/or stiffness values as their heavier counterparts [2]. Hence, it could be valuable in facilitating the reduction of part weight and quantity, which would result in a lowered cost and better fuel economy along with increased part performance and reliability [3,4].

Within the military community, the use of AM can be advantageous in many of their applications. A notable one being the exploration of AM's use for unmanned aerial vehicles (UAVs), specifically for improving structural and aerodynamic efficiencies [5]. Many of these UAVs also employ an IC engine, which is seeing an increased emphasis in the use of AM to improve engine designs [6,7]. Since military vehicles are typically produced in low quantities as compared to the consumer market, AM becomes a more economical alternative to traditional manufacturing methods. Even in some cases higher quantities still show cost savings, as proven by Laureijs et al. when considering both the manufacturing costs and the resultant fuel savings of an AM optimized engine bracket to the forged original [8]. Additionally, AM only requires the storage of the build files and powder to re-make parts. Therefore, there would be a reduced need for over production of critical spares, along with no longer needing to store them and their molds or dies. AM can have a faster lead time when manufacturing a new part in small quantities since it is not dependent on the creation of a machine program or the design and manufacture of an expensive mold when one is not readily available [9]. Finally, AM is more robust and flexible to differing sizes and geometries. Thus, one-off setups are no longer required, and the same machine that can manufacture a simple bracket can also fabricate an engine block, as long as it fits within the build envelope [10].

As a result of its potential advantages, this effort will discuss the

* Corresponding author at: 3144C Learned Hall, 1530 W. 15th Street, Lawrence, KS 66045, USA.
E-mail addresses: jamee.d.gray@gmail.com (J. Gray), depcik@ku.edu (C. Depcik), jennifer.m.sietins.civ@mail.mil (J.M. Sietins), Andelle.kudzal@navy.mil (A. Kudzal), rrogers@udel.edu (R. Rogers), kyu.c.cho2.civ@mail.mil (K. Cho).

https://doi.org/10.1016/j.jmapro.2023.04.054
Received 16 March 2022; Received in revised form 24 April 2023; Accepted 24 April 2023
Available online 3 May 2023
1526-6125/© 2023 The Author(s). Published by Elsevier Ltd on behalf of The Society of Manufacturing Engineers. This is an open access article under the CC BY-NC-ND license (http://creativecommons.org/licenses/by-nc-nd/4.0/).

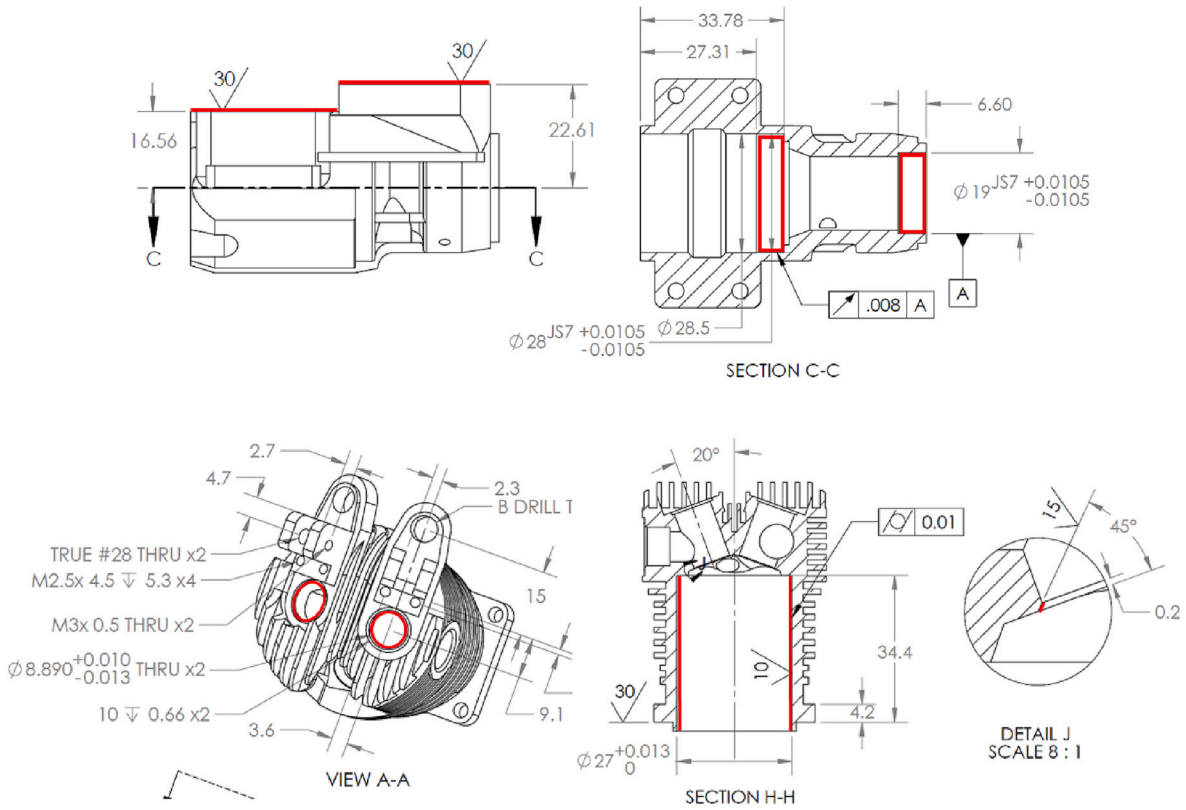

Fig. 1. Crankcase (top) and cylinder head (bottom) drawing section views with critical areas highlighted red, units in mm. (For interpretation of the references to colour in this figure legend, the reader is referred to the web version of this article.)

entire AM process while employing laser powder bed fusion (LPBF) and the difficulties that come with utilizing this technology to manufacture IC engine components. The engine chosen for this study was a Saito FG-11 engine, typically used for remote control airplanes. This four-stroke, 10.6 cc, spark-ignition, IC engine uses a 20:1 mixture of regular gasoline and two-stroke oil [11]. The parts that make up most of the weight are the cylinder head and crankcase; hence, these components can benefit the most from using AM and were chosen for this analysis. The goal was to compare the stock Saito FG-11 engine to the AM version.

2. Materials and methods

First, the materials and machines employed are discussed while factoring in the flexibility that AM allows for lightweight components. In many military applications there might not be a drawing associated with the broken part (e.g., it has been lost or not filed) and even less likely a corresponding Computer-Aided Design (CAD) file, hence, reverse engineering is an essential tool. This can control the costs of replenishing spares and plays such a prevalent role in military applications that there is a MIL-HDBK outlining the guidance and procedures for it [12]. As a result, the subsequent section describes the process of reverse engineering the cylinder head and crankcase while paying critical attention to high tolerance areas. Then, in preparation for metal LPBF additive manufacturing process, these CAD files were modified for orientation and support to generate accurate structures while (ideally) preventing delamination. Finally, the part locations on the build plate are provided with the goal of minimizing spatter and wear on the blade/roller of the recoater.

2.1. Material determination and machine choice

The stock Saito FG-11 engine is of a die cast aluminum (Al) design and through a Vickers hardness test along with the use of a handheld X-ray fluorescent (XRF) gun (79.39 % Al, 17.35 % silicon (Si), and 1.81 % copper (Cu)), the specific alloy of aluminum identified was Al 390 [13]. Since this material is not available for use with AM, two other material options were considered for the crankcase and cylinder head: Ti64 and AlSi12. Investigating heat transfer parameters finds that Ti64 has lower coefficients of thermal expansion and conductivity (8.6×10^{-6}/C and 6.7 W/m·K), respectively, as compared to 21.5–23.6 $\times$ 10^{-6}/C and 130–222 W/m·K for aluminum [14]; hence, operation of the engine could be affected when employing Ti64. Since the crankcase will not encounter a significant amount of heat from the combustion process, Ti64 was chosen for this component due to its respectively high specific strength (203.16 kN·m/kg) that would allow for future optimization efforts [14]. Later results confirmed this hypothesis, with the AM Ti64 crankcase giving values only 10 °C higher than the stock engine [15].

The use of Ti64 for the cylinder head is more complicated. It would be advantageous for combustion by promoting higher temperatures and greater thermal efficiencies [16]. However, the difference in material properties would require a larger cylinder bore to prevent seizure with the Al piston once components are at their operating temperature (OT). This would influence the initial combustion event possibly preventing sufficient compression at lower temperatures while additionally causing increased blow-by past the piston until the engine has achieved a steady-state OT. In addition, if the bore is not made wide enough, the enhanced temperatures seen when using Ti64 could promote the pre-ignition (aka knock) phenomena. This engine is fuel cooled (i.e., lubricating oil is added to the fuel) and higher temperatures could negatively impact engine lubrication and cooling, subsequently putting the engine at risk for thermal runaway. These effects could be mitigated through an optimized heat transfer design, which is part of future efforts. Finally, Ti is prone to galling (i.e., tearing of material under friction); whereas, the high Si content in the Al powder provides additional wear resistance and allows for the elimination of a cylinder liner; thereby, reducing weight and complexity [17,18]. Considering all these factors, when coupled

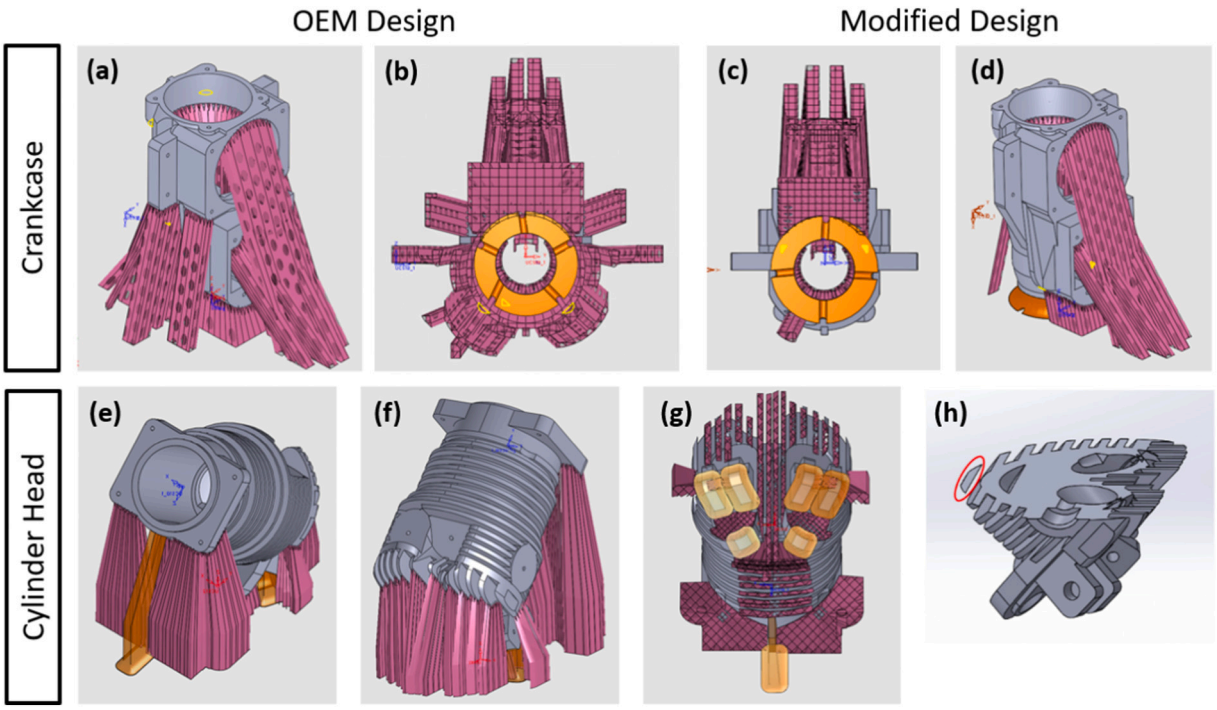

Fig. 2. Support strategies for the OEM design crankcase (a and b), modified crankcase design (c and d), and cylinder head (e, f, and g) with solid and wall supports depicted with orange and pink, respectively, with an example of an unsupported overhang area where support was necessary (h). (For interpretation of the references to colour in this figure legend, the reader is referred to the web version of this article.)

with un-optimized engine components, the complications resulting from using a Ti64 cylinder head are not worth the benefits it would provide; therefore, AlSi12 was chosen.

Machine choice for each part was based on availability and material compatibility. Although LPBF was not the only metal AM machine technology available for this project's use, others such as E-beam and Directed Energy Deposition are not able to provide the same level of accuracy for the size of these components [1,19]. Moreover, LPBF's use is rapidly spreading in the aerospace and energy industry [20,21], giving more weight to the use of this technology for this effort. In general, the choice of a laser or electron powder bed process should factor in the reflectivity, absorptivity, and heating aspects of the selected material [22,23]. Here, the materials available on site along with ready-access to machines with the proper capabilities made the choice more straightforward. The build envelope was not a deciding factor because these parts were small enough (~75 × 50 × 50 mm) to fit in most metal LPBF systems. Additionally, the laser spot size was not considered since neither part had features with <0.3 mm thickness, which would necessitate the use of a smaller laser spot size [24,25]. This is needed for small features since they can achieve smaller melt pool widths while maintaining the same penetration depth required by the layer thickness [25]. The differences in the spot sizes between the machines can also be compensated through the laser parameters used in the build slice file (e.g., hatch spacing, speed, and power used) [25]. For the crankcase, the 3D Systems ProX DMP 320 was used; this machine has a build volume of 275 × 275 × 420 mm, a 500 W laser with a spot size of 80 μm, and uses a hard recoater blade to sweep powder over the build area once per layer [26]. The cylinder head was printed on the 3D Systems ProX DMP 300 which has a build volume of 250 × 250 × 330 mm, a 500 W laser with spot size of 75 μm, and uses a roller recoater that travels across the build area twice between each layer (across and back into position) [27]. Because the roller slightly compacts the powder, this machine is less forgiving of fine or poorly supported features, and in turn, they are likely to result in build failures [28,29].

2.2. Reverse engineering and model preparation

Using caliper, telescoping gauge, and micrometer measurements along with inferences based on the bearings and screws used, CAD models were generated for both parts in SolidWorks. Typical metal LPBF machines are not capable of producing relatively high tolerances. For example, 3D Systems claims a minimum accuracy of 50 μm for their ProX DMP machines [28]. As indicated later, this is not always the case due to variations in machine parameters, build strategies, geometries, and how the build is setup or supported. Therefore, it was crucial to identify critical tolerance areas for both parts, such that material could be added for later post machining.

For the crankcase, these areas were the two inner bearing surfaces highlighted in Fig. 1, which both required a JS7 fit that equates to a tolerance of ±0.011 mm [30]. Keeping these bores concentric was essential for balanced engine operation; otherwise, the vibration induced could have destroyed the engine. Hence, the runout cannot exceed ±0.008 mm [31,32]. Moreover, meshing of the cam gear and crankshaft along with the alignment of the piston connecting rod and the crankshaft journal was important to ensure the cam gear was rotated so that the valves opened and closed appropriately while keeping the crankshaft from experiencing excessive bending forces. Therefore, the heights of the upfacing gasket faces were specified to within ±0.08 mm. To ensure proper sealing of the engine components and to prevent leaks, the gasket faces had surface finishes of around 0.67 μm Ra [33]. As a reference, the measured as-AM surface roughness values were 7.47 μm and 22.28 μm Ra for Ti64 and AlSi12, respectively. The location (depth) of the larger bearing surface was important to ensure the crankshaft was in the correct location allowing the piston to line up with the cylinder, requiring it to have a ± 0.08 mm tolerance. It was also important for all threaded holes on these surfaces to be placed correctly so that the cylinder head and cam gear lined up with the crankshaft in the x and y directions. Thus, a ± 0.08 mm tolerance was placed on those locations. Finally, all other tolerances were kept within ±0.5 mm as to not hinder clearances or allow for excessive removal of material, which would lower the safety factor.

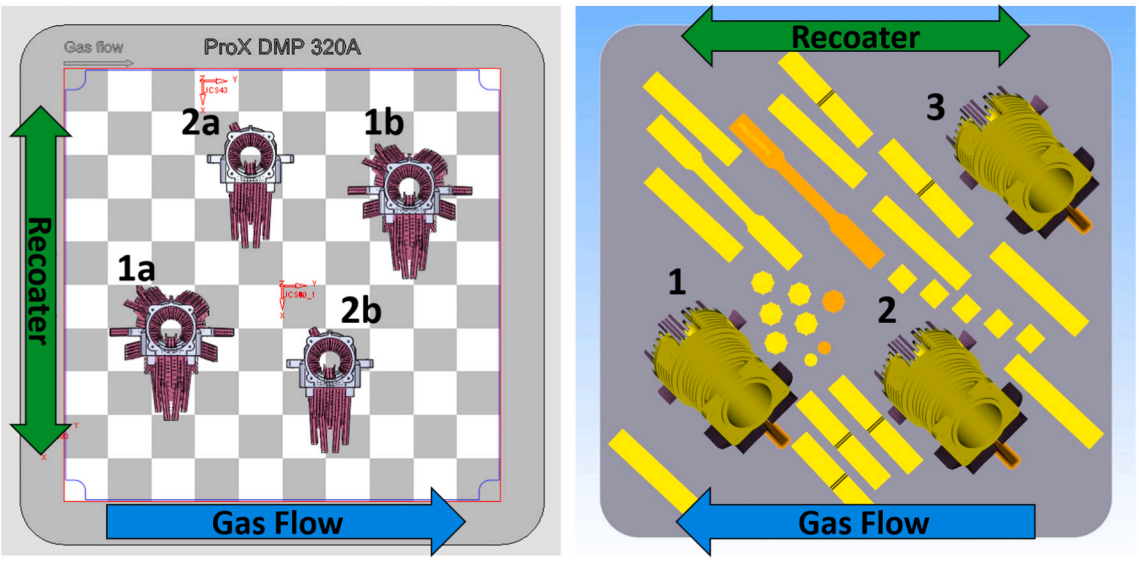

Fig. 3. Build plate arrangement for the OEM and modified design crankcases 1a, 1b, 2a, and 2b, respectively (left) and cylinder heads 1, 2, and 3 (right).

Table 1
Machine parameters for each part.

	Component	Layer thickness [μm]	Laser power [W]	Laser speed [mm/s]	Hatch spacing [μm]
Crankcase	Part	60	50	400	82
	Solid support	60	340	2000	100
	Wall supports	60	150	1600	100
Cylinder head	Part	40	225	1200	70
	Solid support	40	400	2500	70
	Wall supports	40	100	1600	70

For the cylinder head, the cylinder wall needed special attention. The goal was to not use a cylinder liner; thereby, reducing complexity and the number of parts for the engine (an advantage of the AM process). A complex multi-step honing procedure was required to give the necessary surface finish for the piston rings to seat and prevent wear (explained later) [17]. Additionally, the valve guide bores needed to have a 0.05 mm interference fit (red circles in Fig. 1) to retain the brass guide due to differences in thermal expansion at operating temperatures. This interference fit also ensured efficient heat transfer from the guide to the cylinder head [34,35]. Moreover, the chamfer where the valves seat at the top of the cylinder required consideration to ensure that they sit flat and provided an air tight seal so the cylinder can hold pressure for combustion (right depiction in Fig. 1). To obtain this feature, a 0.38 μm Ra surface finish was achieved [36]. As previously stated, the holes for the screws to attach the cylinder head to the crankcase were aligned with a ± 0.08 mm tolerance, and all other tolerances were kept within ± 0.5 mm.

Because AM is reliant on support structures, any overhanging or downskin areas are prone to distortion [37,38]. To prevent this, all holes were filled to a 1.27 mm diameter to become pilot holes for later machining. Additionally, since AM cannot achieve the surface finishes or tolerances necessary for gasket faces and bearing surfaces, 0.76 mm of material was added for subsequent machining. Furthermore, 1.27 mm was added to the cylinder head walls in case porosity occurred just below the surface, as this is more likely if the border parameters are not optimized to prevent keyholing porosity.

2.3. Part orientation and support design

For metal LPBF, AM supports are necessary for attaching the part to the build plate and for overhanging areas that have a $<45^{\circ}$ angle to the build plate with an area > 2 mm^2. Solid supports are important in providing structure and preventing delamination. In addition, they act as heat sinks during the AM process, aiding in the reduction of the residual stresses (particularly for Ti64) that build up due to thermal history [24]. The first step in designing the supports is determining the orientation of the part with respect to the build plate. Usually, this decision is based on minimizing part height to reduce build time and reducing overhanging areas to decrease the need of supports that can cause poor surface finishes and increased post-processing [37,38]. Supports for both the crankcase and cylinder head were designed within 3DXpert.

For the crankcase, critical areas in need of support reduction were the internal features (particularly the bearing surfaces) since they would be difficult to remove and then machine to a smooth surface. Therefore, the part was printed vertically with the propeller end facing down, which only required one internal support. All outside supports were angled away from the part to allow them to be more readily removable (Fig. 2). An alternative design modified for AM was created to minimize the need of supports and reduce the amount of post-processing. This was done by simplifying the outer geometry and eliminating many overhanging areas (Fig. 2). Due to these changes, the support volume was reduced from 7.55 cm^3 to 5.49 cm^3 and the overhanging area reduced from 1506.1 mm^2 to 1094.5 mm^2. However, the volume of the crankcase itself did increase from 30.27 cm^3 to 33.08 cm^3. Perforated wall (2 mm square grid pattern, and 2.5 mm tall top teeth) and solid supports were used. The solid support used the skirt option to create a fillet and drain holes were added to help alleviate stress buildup on the plate.

Regarding the cylinder head, the internal geometry at the roof of the cylinder made selecting a print orientation difficult. Since these surfaces are complex, post machining was not possible. This meant the only orientation choice was to angle the cylinder head upside down and at 45° where the spark plug surface was not in need of support while also keeping the build symmetric (Fig. 2). This prevented supports from being necessary inside the cylinder or between the fins that would have been nearly impossible to remove. With this slice orientation, the fins would be starting completely unsupported since they would not be connected to the cylinder itself initially (Fig. 2 far right). Because of this, a support was added at the underside of every fin. This choice resulted in

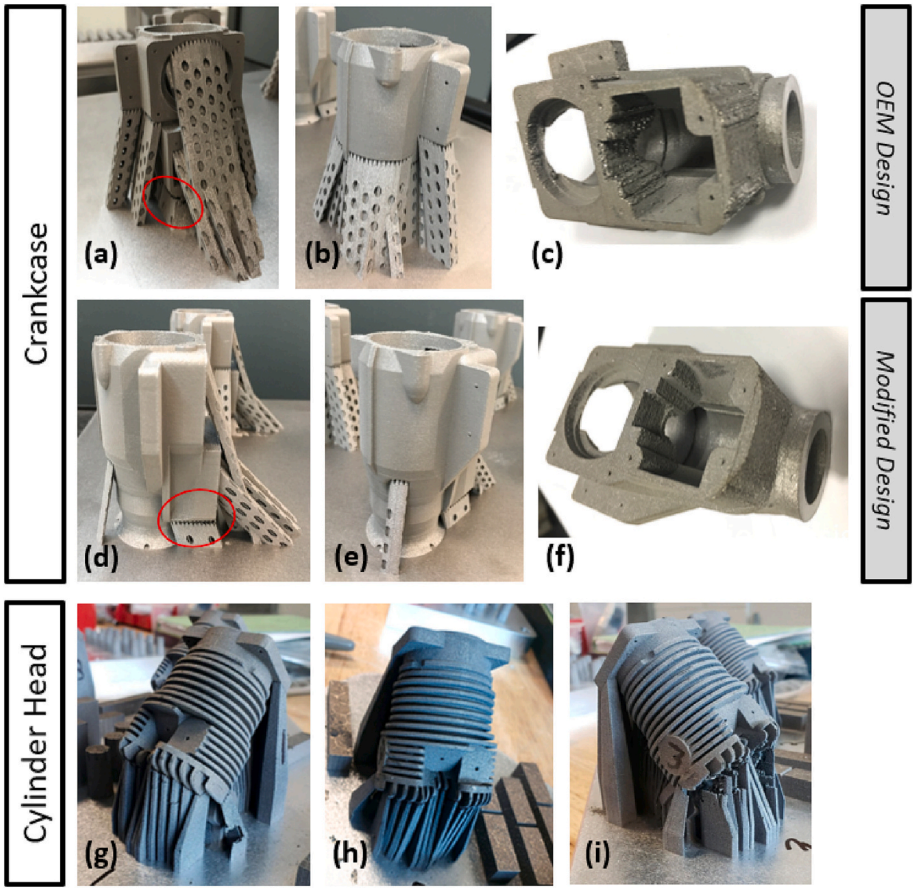

Fig. 4. On-plate AM build results for the OEM design crankcase (a and b), modified design crankcase (d and e), cylinder head 1(g), cylinder head 2 (h), and cylinder head 3 (i); results after plate and support removal are also depicted for OEM design (c) and modified design (f) crankcases.

Table 2
Crankcase and cylinder head porosity results- comparison of cast and AM parts.

	Machine	Voltage [keV, uA]	Voxel size [μm]	Total porosity volume [%]	Largest pore size [mm^3]
Cast Al crankcase	Zeiss	160, 63	57.36	0.0280	0.3241
AM Ti64 crankcase OEM design average	Northstar	225, 250	41.73	0.0027	0.2779
AM Ti64 crankcase modified average	Northstar	225, 250	41.73	0.0003	0.0082
Cast Al cylinder head	Zeiss	100, 90	57.36	0.1571	9.0730
AM Al cylinder head averages	Zeiss	100, 90	41.79	0.0256	0.0593

a support volume and area of 10.64 cm^3 and 654.84 mm^2, respectively. The supports for the cylinder were slightly more robust than for the crankcase since this part was manufactured on a slightly less forgiving machine (especially with fine features as discussed in the previous section). In this case, the wall support pattern used 1 mm square grid size with no wall texture applied (walls are solid), and 1.5 mm tall top teeth. The solid support style remained consistent with that of the crankcase.

2.4. Build layout and build strategies

After deciding print orientations, setting plate layout was next in the build preparation process. When considering part location, there were two major factors to consider: gas flow and recoater travel directions [39–41]. Large parts should not be placed downstream of the gas flow as spatter could travel to other parts in the build, causing a greater potential for defects. When considering recoater direction, all walls/parts should be angled at 10–80° with respect to the recoater. This helps to reduce wear on the blade/roller and keeps the powder distribution even, reducing potential for multi-part build failures. Parts should be arranged in an offset pattern with enough space between for the same powder spread reasons and to provide better heat dissipation. As a result, two parts of each crankcase design were printed (1a & 1b are the OEM design; 2a & 2b are the modified design in Fig. 3) to allow for error when machining and three cylinders were printed along with mechanical test specimens for other research purposes (Fig. 3).

The final step in the build setup process involved slicing the build file with selected machine/build parameters applied, this turns it into a format that can be loaded and read by the machine. After slicing, the crankcase build came out to be 1220 layers and was predicted to take a total of 12.78 h. The cylinder build included 1862 layers and was projected to take a total of 44.67 h with everything on the build plate (each cylinder contributed 3.68 h). Table 1 provides the parameters used for each component during construction. These parameters were chosen based on past efforts by using the machines over a wide variety of LPBF activities, many of which involved metallographic analysis and mechanical testing for verification. Since porosity and tolerances were not of concern for the support structures, less ideal, but faster parameters were used to speed up the build and allow for easy support removal.

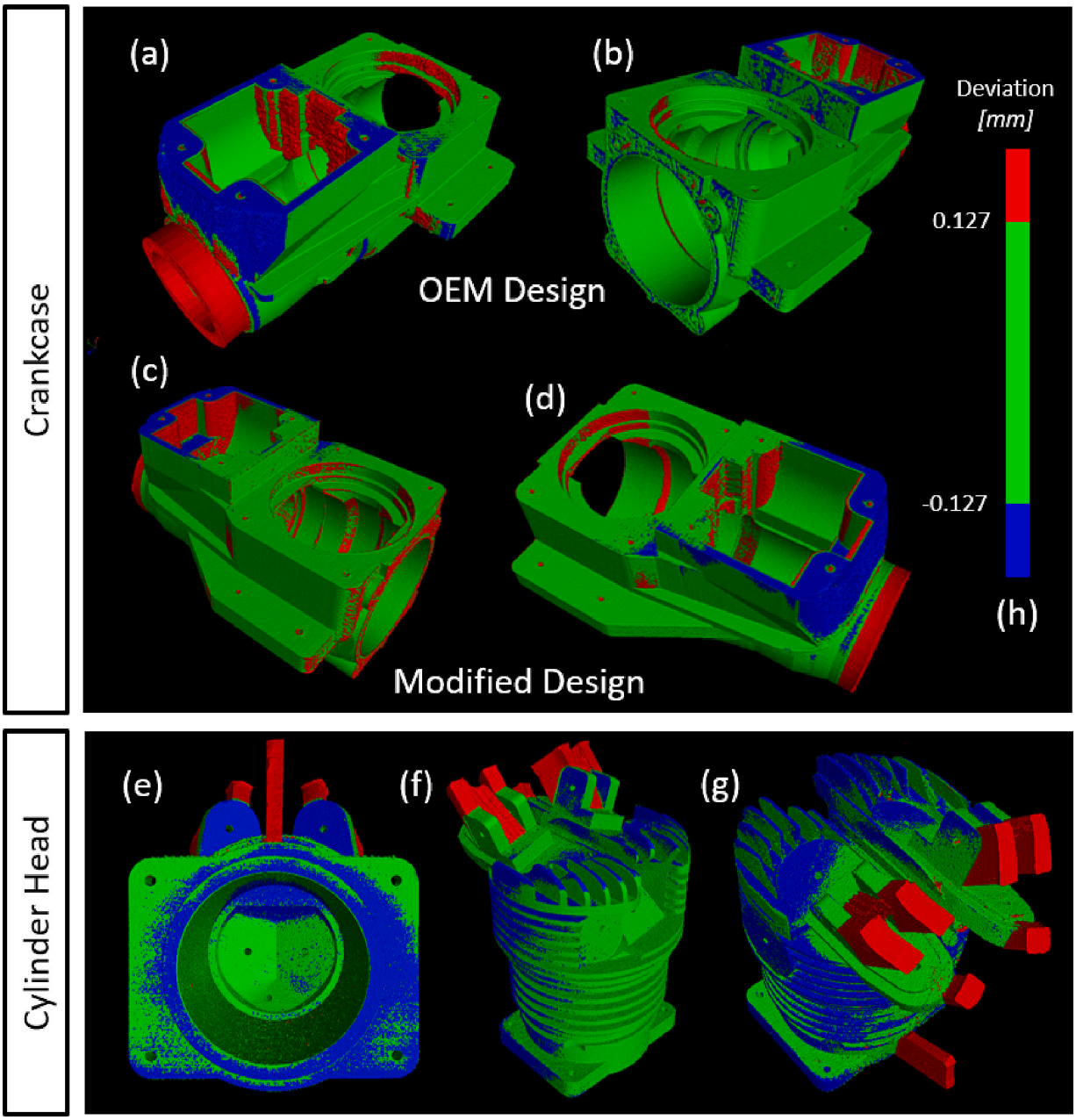

Fig. 5. Nominal and actual dimensional analysis of AM parts vs. CAD files for OEM design crankcase (a and b), modified crankcase designs (c and d), and the cylinder head (e, f, and g), each with multiple views and visualizations based on the values in the scale bar (h).

3. AM results and discussion

The first evaluation of any AM-constructed part involves a visual review of the structure. Areas of delamination were noted and reviewed to ensure general acceptance or non-acceptance of the printed parts. Next, a quantitative analysis was accomplished to confirm that the parts are within acceptable tolerances or that out-of-tolerance areas would not impact operation or possibly lead to failure. Subsequently, reviewing part porosity helps supply insight where fatigue cracks might occur and potentially information about the life of the part. Finally, the resulting defects are found prior to preparation for engine testing.

3.1. Visual review

Fig. 4 presents the build results of the two crankcase designs, circled in red are the areas where the part delaminated from the support structure. Regarding this outcome, Zaeh et al. demonstrates through AM bar simulations that the residual stress produced between the support and the structure is respectively larger than those in the part or the support themselves, which is why delamination in this area is more likely [42]. The circled delamination in the figures likely resulted from the buildup of residual stress. The smaller cross-sectional areas between the upper teeth of the support and their attachment to the part are inherently weaker. When investigating the support areas after removal, it should be noted that the modified design had a relatively cleaner resulting surface. In comparison, the OEM design had significant unconsolidated powder built up in these areas. This build up is most likely due to the additional supports surrounding the part, preventing the heat from dissipating (i.e., acting as an insulator) and subsequently producing higher temperatures. This caused the laser to partially melt the layers beneath the supports and surface. This poor finish could also be a result of an increased amount of ejecta caused by the larger lasered area

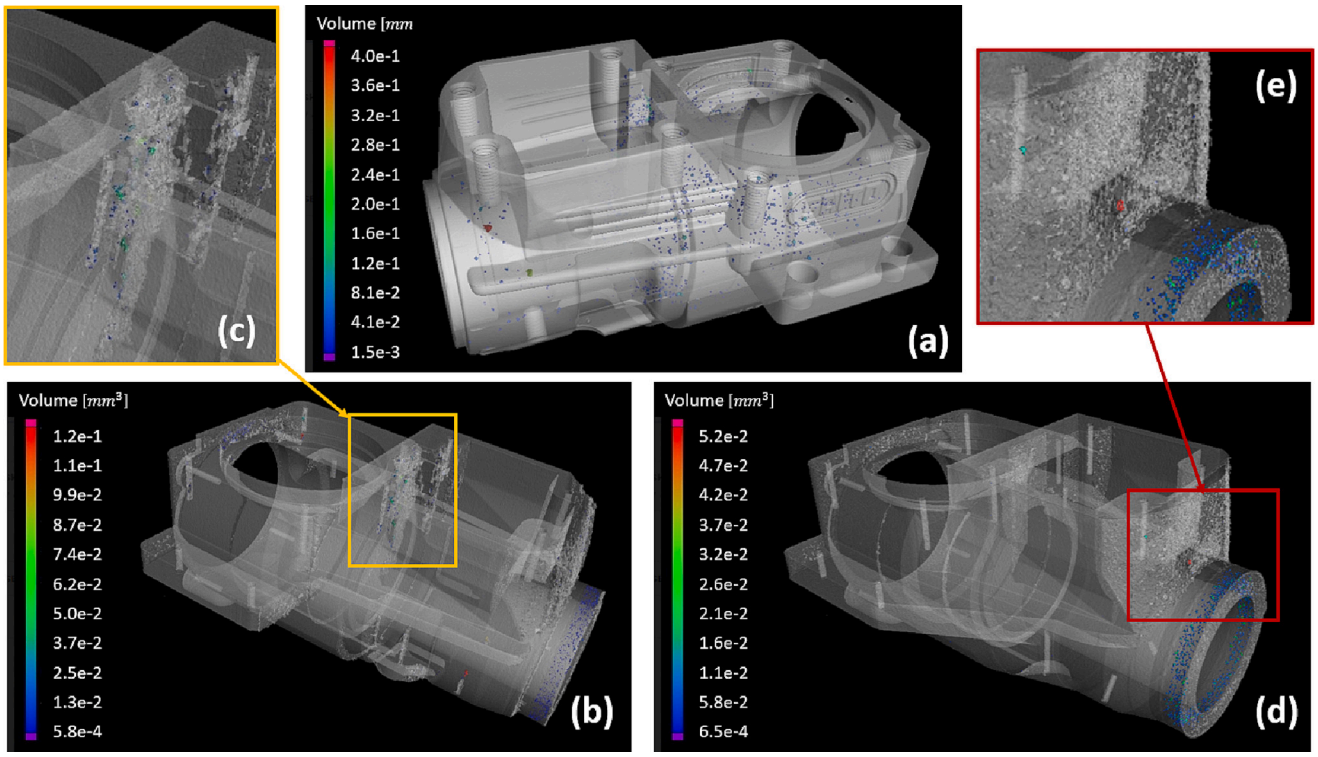

Fig. 6. Visual representation of porosity in die cast crankcase (a) vs. AM crankcase 1a OEM design (b) with close up of high porosity area (c), and AM crankcase 2b modified design (d) with close up of high porosity area (e).

(due to additional supports) being thrown in the central area of the surfaces [43]. Besides these areas, the support structures were removed relatively easily by hand with pliers, whereas, the solid supports required a milling process.

Fig. 4 also displays the results of the cylinder head AM process using the ProX DMP 300 machine. These images show almost no delamination, and they exhibit mostly intact supports. However, the third cylinder head had significant support cracking and damage. This is likely a result of not having tensile test bars on both sides of the cylinder acting as a barrier to prevent the powder or supports from shifting when the roller adds a new layer. This reason is why lattice structures and other fine features often have walls printed around them. After removal of the supports, this lack of protection had a notable effect on the quality of the upper fins.

3.2. Dimensional analysis

To decide whether these parts were useable, a nominal/actual dimensional analysis was performed with the AM part compared to the CAD file. A Zeiss Xradia 520 micro-CT was used to analyze the AM cylinder head; whereas, the AM crankcase was scanned using an Northstar X-5500 system (voltage and voxel settings are listed in Table 2) due to the increased density of the Ti64 that hindered transmission of the X-rays and required a higher scanning voltage than what the Zeiss micro-CT could provide. Fig. 5 shows the original and modified designs for the AM crankcases and the cylinder head, respectively, as compared to their CAD models. In these figures, everything in green is within 0.127 mm, which is typical milling tolerance [44]. The blue areas show where material is missing and the red areas highlight extra material present. The blue areas on the front of the crankcase were a result of the delamination mentioned previously, which will cause the front thicknesses to be slightly thinner after the part was machined. Many of the red areas on both parts were caused by the leftover support areas that were later machined.

It is important to note that although there were areas out of tolerance, most of these areas were post machined or they were determined to not be of critical importance for successful engine operation. For example, even though the front blue areas in the crankcase were thinner than intended, this is not a highly loaded area; hence, it should not have hindered the lifespan of the part or changed its performance. Likewise, almost all internal features were bored, and any surfaces left untouched were not critical because they still allowed for clearance of moving engine assembly components. Even though many of the fins on the cylinder head were slightly off, they should have only had a minor effect on heat transfer. A considerable number of blue areas were a result of the corresponding AM machine's achievable tolerance. Overall, these parts were deemed to be within acceptable ranges.

3.3. Porosity results

To obtain an understanding of the baseline porosity level in these engine components, the die cast part CT scans were analyzed using both Volume Graphics and a Bruker CTAnalyzer (CTAn) macro developed following the efforts of Sietins [45]. It should be noted that threshold segmentation levels were set visually; thus, leaving some room for user bias, and all volumes <0.0002 mm^3 were classified as noise based upon the scan resolution. Figs. 6 and 7, along with Table 2 display the results for the die cast crankcase with the spikes in porosity percentage directly correlated to material thickness. The main material defect observed in the die cast components is the porosity caused by micro-shrinkage and dissolved gases during solidification [46,47]. This porosity can stem from hydrogen content and local freezing rate along with the local temperature gradient potentially playing a role [46,47]. Since the porosity in this case correlates with thickness, it can be assumed that the culprit was non-ideal cooling during the casting process. This is an issue with this process since it is expensive to develop dies to ensure a uniform cooling event for complex parts such as ones with varying thicknesses [48]. Because of this, for relatively inexpensive parts, it makes sense to keep the thicknesses consistent throughout the part to alleviate any potential porosity issues.

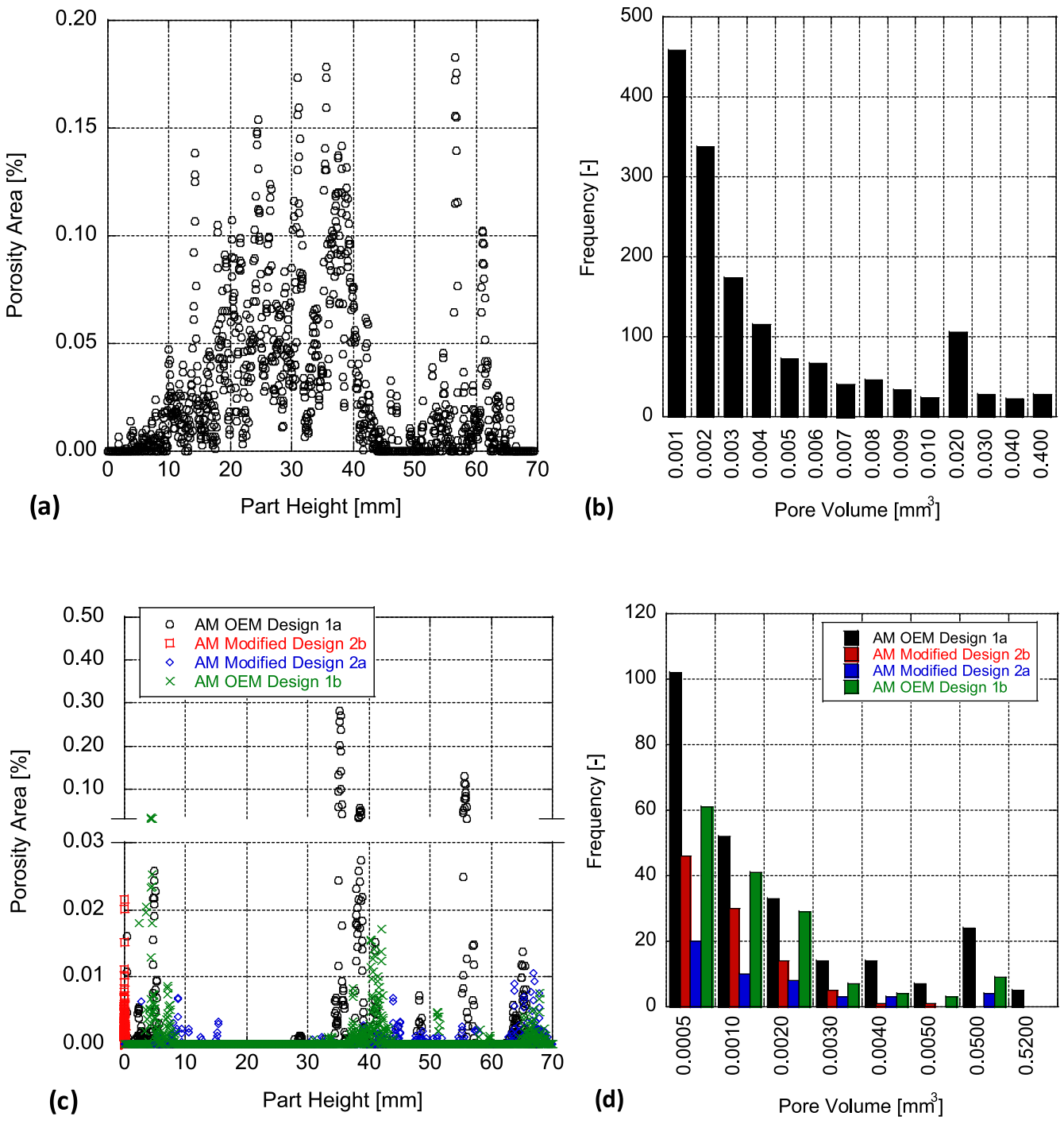

Fig. 7. Porosity area percentages and pore size distributions for die cast (a and b respectively) and AM (c and d respectively) crankcases.

Once a baseline was decided for the die cast parts, the AM parts were then analyzed as illustrated in Fig. 6. It should be noted that the area at the front of the crankcases with noticeably more blue porosity is contained within the solid support structure and was not included in the quantitative analysis. As indicated before, Ti64 has a higher density; hence, a higher energy CT scanner was used, but the voxel sizes of the die cast crankcase and the AM scans are similar, meaning valid comparisons can still be made.

The spikes in porosity in Fig. 7 are about 0.1 % higher in the AM original OEM design parts (1a and 1b), but (like discussed before) these were a result of the leftover support areas and were machined. This also explains why one of the AM OEM design parts (1a) has its largest pore size at almost double the die cast part, but the other AM OEM design (1b) has the largest pore size 1/10th of the die cast part. Otherwise, the porosity stays relatively consistent and has an average percent porosity area of 0.0027 % and 0.0003 % for the OEM and modified designs which are approximately 1/10th and 1/90th the average of the die cast part.

Building on this, the modified design results are better (2a and 2b). The porosity present is only from support areas, and the largest average pore size is 1/34th of the AM crankcase OEM design. Comparing image slices of the crankcase versus the solid support show that this negligible porosity was not a result of the image quality and that the scans were still picking up notable porosity in the support structure. Direct porosity comparisons are presented in Table 2. These results appear promising

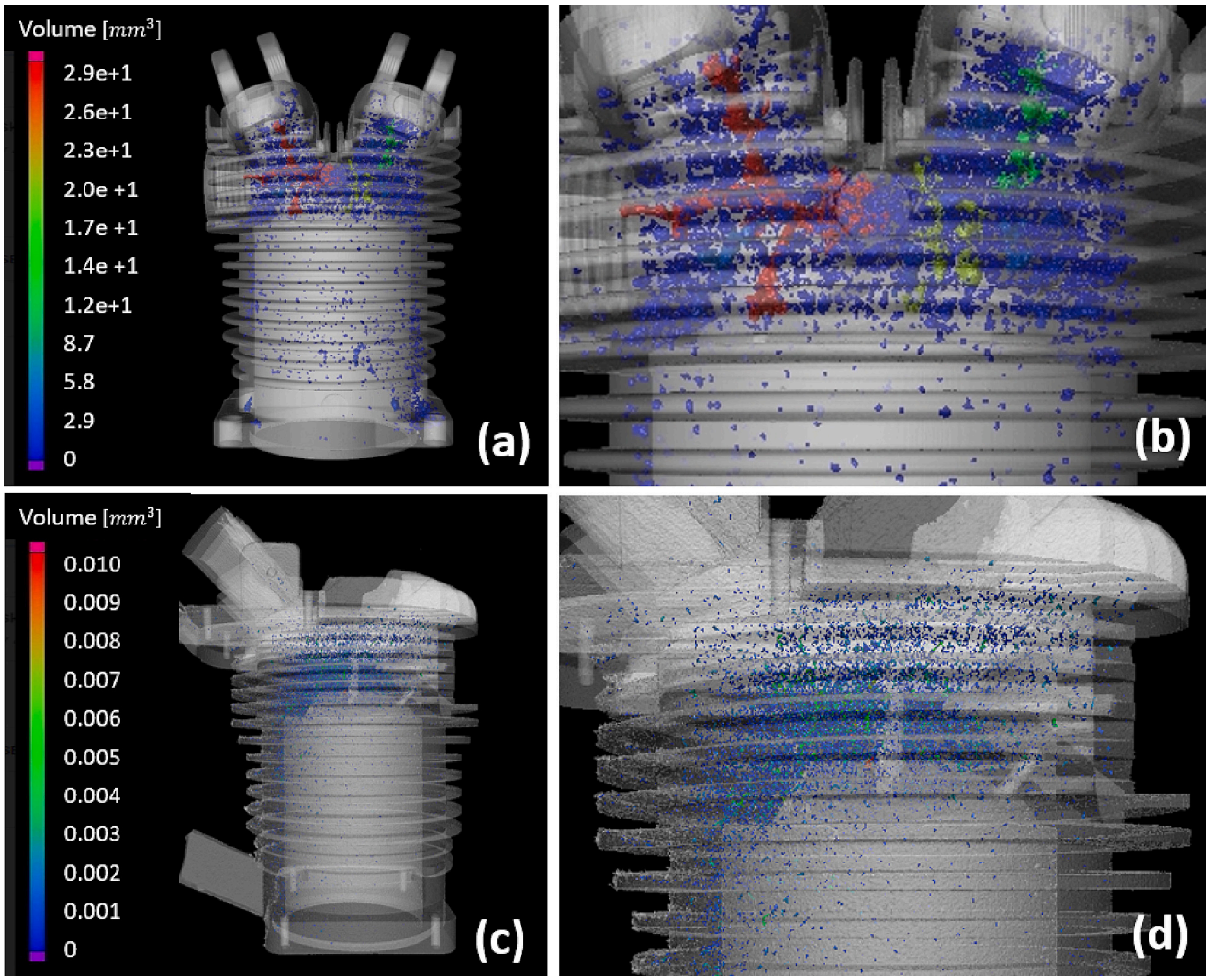

Fig. 8. Visual representation of porosity in a die cast cylinder head (a) with a close-up view (b) vs. the porosity in an AM cylinder head (c) with a close-up view (d).

since Mayer et el. demonstrated that 98.5 % of fatigue cracks initiate at porosity [46] while Major et el. found the greatest influencer on fatigue life was the largest pore size [47].

For the cylinder head, the same porosity analysis procedure was followed. Unsurprisingly, the die cast cylinder head had a higher porosity than the die cast crankcase because of its thicker material areas at the top of the cylinder (Fig. 8). Specifically, the red, green, and yellow areas are a result of the large pores found. Overall, the cylinder head's largest pore size and total porosity percentages were roughly 30× and 5× greater than the cast crankcase, respectively (Table 2).

In general, the porosities of the AM cylinder heads are 0.0229–0.0253 % higher than the AM crankcase designs. Comparing the die cast cylinder head and the AM version still indicates a positive trend with the AM cylinder heads having an average porosity area percentage of 0.0256 % as compared to 0.1571 % for the cast part. The cast cylinder head had large pores that were about 150× greater than the AM parts, resulting in the bigger porosity area percentage (Table 2). When seeing the pore volume distribution in Fig. 9, the AM parts had considerably more pores that were smaller than 0.001 mm^3 (roughly 3300 and 1350 for the AM and die cast, respectively). This increase in small pores could have influenced the surface finish; thereby, making the use of a cylinder liner necessary. It can also be observed that these small pores are more prevalent on the backside of the cylinder head (Fig. 8) since this side was downfacing during the build process.

3.4. Resulting defects

A current weakness of the AM process is its ability to create clean features, especially sharp corners. When combined with a residual stress build up, corners are prone to produce localized stress concentrations and cracking is more likely to happen [49,50]. Fig. 10 illustrates a crack that occurred along a corner feature on this part with this defect occurring in crankcases 1a and 2a. These parts were approximately in line with each other with respect to the recoater direction and were both upstream of the other two parts regarding cover gas flow. As a result, either of these locational variables could have potentially contributed to producing the defect in both parts. Investigating, crankcase 1a had a crack depth of 1.47 mm and length of 15.05 mm; whereas, crankcase 2a had a crack depth of 1.89 mm and length of 12.20 mm. These defects were concerning due their proximity to one of the major cyclical loading areas induced by the bearing during engine operation when the piston is at top dead center and bottom dead center. This is concerning as Akgun et al. and Mian et al. both demonstrated a reduction in fatigue with AM Ti64 when there are defects, such as pores or cracks, with surface defects having the most detrimental effect [51,52]. While the AM crankcases did show less porosity, the surface defect cracks found likely render these parts unusable, given the cyclical loading nature of their application. Because of this, crankcases without this defect were used going forward in the machining and testing processes. In addition, Fig. 10 provides a closer look at the unconsolidated powder experienced in the original crankcase designs. The wavy structure on the surface is the leftover support and the darker gray is the unconsolidated powder.

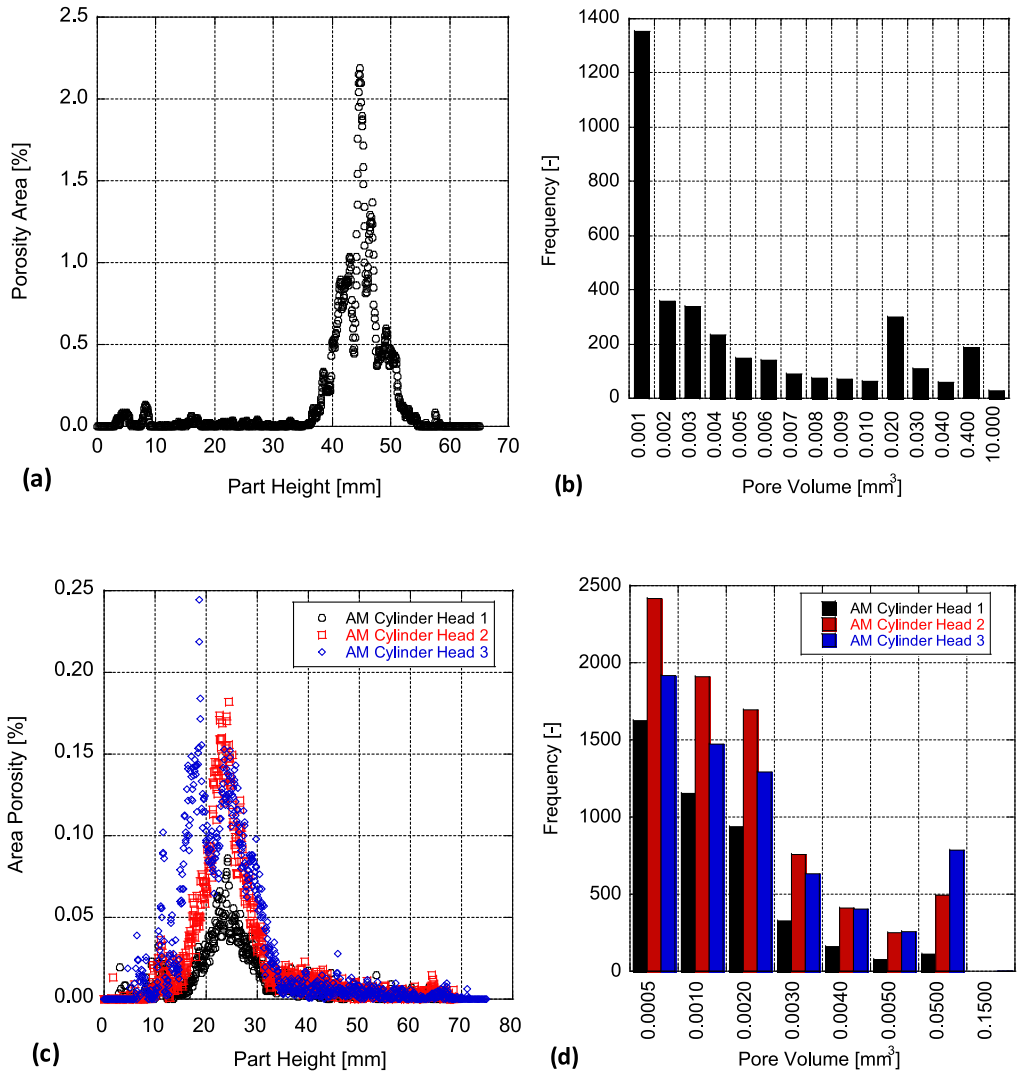

Fig. 9. Porosity area percentages and pore size distributions for die cast (a and b, respectively) and AM (c and d, respectively) cylinder heads.

The AM cylinder heads had a small defect (0.51 mm) resulting from the geometry, creating a localized stress concentration. The material thickness in this area was respectively low and there were two corners close to each other making this flaw possible. This defect was seen in all three of the manufactured cylinder heads. As a result, the quality of the fins and features were investigated visually to decide which would be best for testing going forward and cylinder head 2 was chosen.

4. Post-processing results and discussion

Given the cyclical loads, high pressures, and fast engine speeds encountered in internal combustion engine operation, post-processing the printed AM parts is a key component in ensuring their successful operation. This includes removing residual stresses, properly machining parts to their final tolerances, and honing the cylinder.

Residual stresses are caused by non-uniform cooling and can result in unfavorable conditions such as cracking, or loss of compressive yield strength [53]. It is important to remove these stresses using a heat treatment process. With respect to Ti64, these residual stresses are especially detrimental due to its poor heat dissipation [54]. The process for Ti64 stress relief was as follows and occurred in an inert environment using Ar: 1. The temperature was raised to 600 °C in 1 h; 2. Dwell for 4 h; 3. Cooled at 6 °C/min for 1 h 40 min; and 4. Part was removed [53]. The results of this stress relief process should bring the stress down from upwards of 750 MPa to something close to negligible [53,55]. Similarly, heat treatment was investigated for the cylinder head to obtain a comparable hardness and yield strength to cast Al. However, the absence of Mg in AlSi12 results in the elimination of any phases to precipitate out for strengthening. Therefore, heat-treating can degrade the properties as indicated in a report by the U.S. Army Research Lab [56]. As a result, a choice was made to not heat treat the AM cylinder head.

After undergoing the heat treatment processes, the wall support structures were removed manually using pliers. Then, a band saw was used to detach each part from the build plate by sawing through the solid support structures. This is also commonly done with wire Electrical Discharge Machining. Lastly, the parts were CT scanned and checked for distortions, porosity, and cracking to ensure they were usable before undergoing the final required post machining process. Fig. 11 outlines all surfaces and features that required machining to achieve the final form of the crankcase and cylinder head. Since the cylinder head was made of aluminum, special care was taken during the fixturing process as to not yield the material by crushing it in a vice, which would cause the inside walls to lose cylindricity and/or potentially damage the fins. As a result, two fixturing aids were developed and machined to help with this process. All tools and equipment needed to accomplish this machining can be found in the thesis of the first author along with detailed step-by-step descriptions [15].

Due to the high silicon content of the AM cylinder head, a cylinder

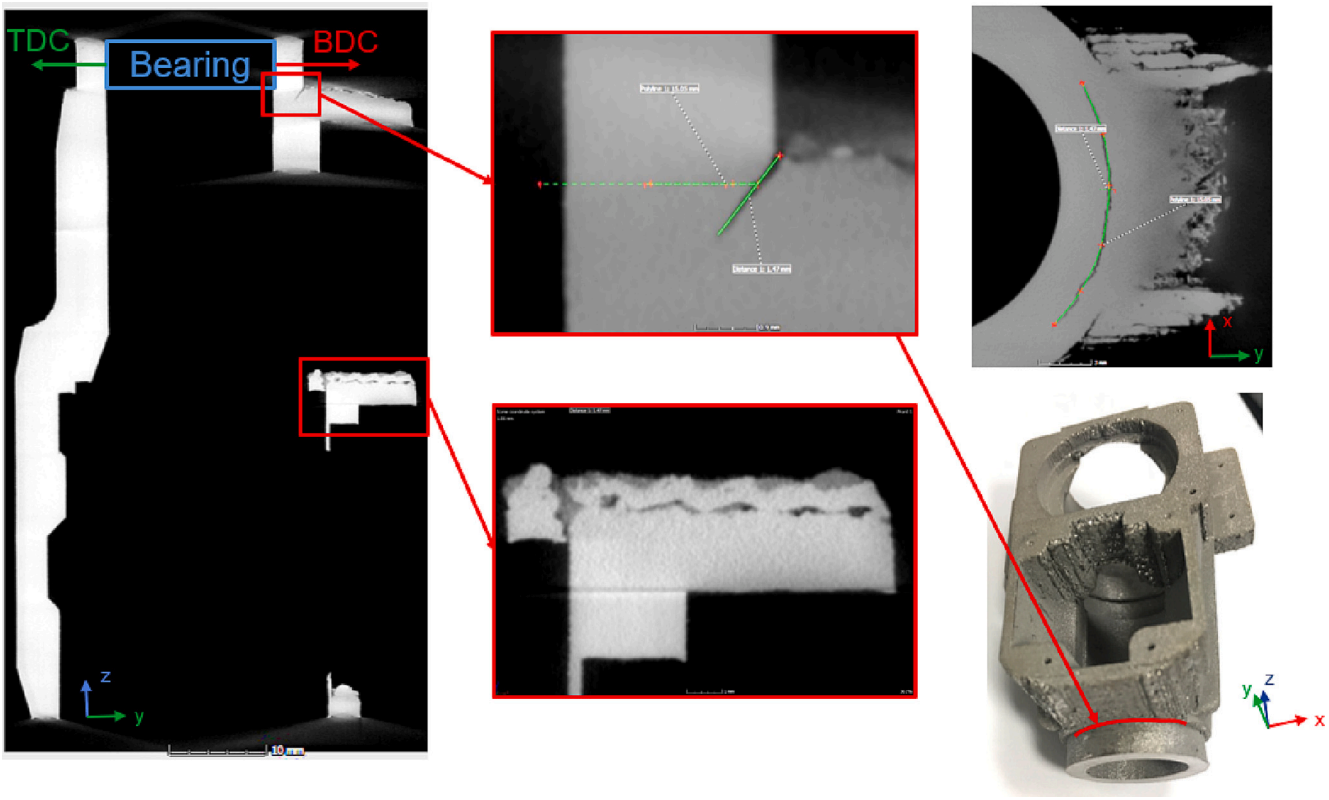

Fig. 10. Crack defect in AM crankcase OEM design 1a.

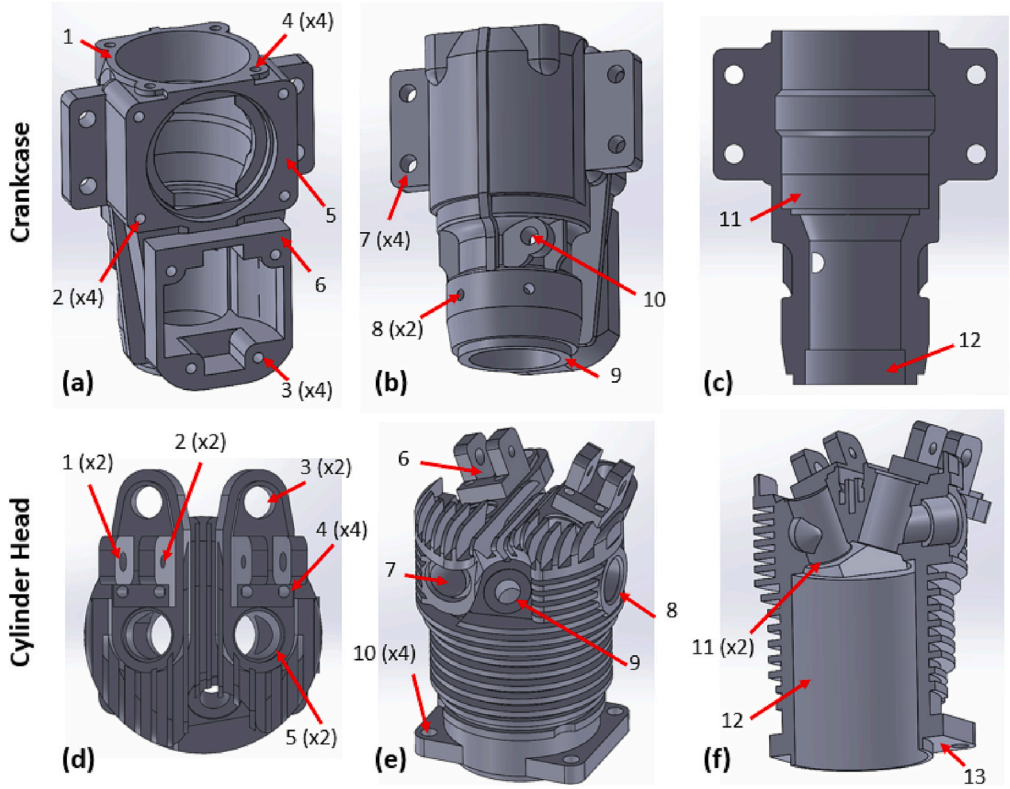

Fig. 11. Surface and feature identification for post-machining on the crankcase's top and back gasket faces and threaded holes (a), that back threaded holes and flange through holes (b), and the internal bearing surfaces (cut view in c), and the cylinder head's external surface features (d and e), and internal features (cut view in f).

Table 3
Roughness value comparisons of cylinder head walls.

Value	Description	Unit	Stock cast part	After boring	After 220 grit	After 400 grit	After polishing	After silicon exposure
Ra	Roughness average	μm	0.173	1.911	1.018	0.288	0.198	0.232
Rq	RMS roughness	μm	0.222	2.364	1.293	0.402	0.257	0.330
Rz	Average max. height of the profile	μm	1.342	11.783	7.845	3.501	1.714	2.338
Rp	Maximum profile peak height	μm	0.502	5.310	2.633	0.927	0.631	0.545
Rv	Maximum profile valley depth	μm	0.840	6.472	5.212	2.574	1.082	1.792
Rt	Maximum height of the profile	μm	1.986	15.251	9.617	5.161	2.811	3.284
Rk	Core roughness	μm	0.484	6.095	3.083	0.795	0.382	0.564
Rpk	Reduced peak height	μm	0.253	2.430	0.929	0.301	0.552	0.258
Rvk	Reduced valley depth	μm	0.442	2.584	1.984	0.779	0.645	0.726
Mr1	Peak material ratio	%	7.39	9.40	5.29	4.94	11.57	8.47
Mr2	Valley material ratio	%	85.95	89.33	85.39	84.11	80.18	83.46

liner was unnecessary and the cylinder was honed according to a hypereutectic aluminum boring process [17,57]. The goal of this process was to achieve a smooth finish with a crosshatch pattern for oil lubrication, and a 0.483 μm silicon exposure height. An advantage of exposing this silicon was that it provides a harder surface for the piston rings to ride on, preventing wear on the aluminum. Before honing, the Sunnen honing mandrel, stones, bronze guide shoes, and felt pads were modified for use in a blind hole. After modification, a plateau finish with exposed silicon was accomplished [15,57,58].

To ensure the honing process was accomplished correctly, a Mitutoyo Profilometer SJ-210 was used to take intermittent surface roughness measurements. Table 3 shows the surface R-values of the stock cylinder head, and between all steps while honing the AM cylinder head. Each of these values is an average of the four measurements taken on the front, back, and sides of cylinder. Diameter measurements (average of three) taken between honing steps at 6 locations using a telescoping gauge and a 25.4–50.8 mm micrometer to characterize the amount of material being removed. Data from this showed that the honing process removed less material from the bottom of the cylinder as compared to the rest of the part due to a slightly elliptical bore geometry, this was later found to be a problem which negatively affected the engine's performance [59]. Additionally, Sunnen provided approximate numbers for where R-values should fall for a “Performance Finish” including: Ra = 0.152–0.254 μm, Rpk = 0.203–0.330 μm, Rk = 0.406–0.610 μm, Rvk = 0.381–0.584 μm, Mr1 ≥ 6 %, Mr2 ≥ 83 %, and Rz = 0.254 × Ra μm [60]. According to these values, the only value that fell outside is Rvk that is still relatively close.

Fig. 12 shows the surface profiles that correspond to each of these steps. As can be seen, these profiles are exactly what was expected: i.e., the roughing stone created peaks and valleys more consistently than boring did, the 400 grit cut off some of the peaks, the polishing stone smoothed these peaks further, and the exposure step produced silicon protrusions roughly 0.483 μm above the surface. When comparing the results of this honing process to the stock cylinder liner (Fig. 12) the AM cylinder has a more apparent plateau finish with deep valleys for oil lubrication. There also was some slight visible porosity in the AM cylinder wall (Fig. 13).

5. Final comparisons and physical test results

Once the engine was fully manufactured, one final CT scan was performed on both parts to check for any cracking or defects that vibration from machining may have caused. It was found that all critical features fell within ±0.127 mm of the stock cast parts, with the only areas out being in spots that would not hinder successful operation. Final porosity percentages of the AM crankcase and cylinder were both approximately 1/25th of the stock cast part porosities (since support material was fully removed). These results showed that the parts were similar enough geometrically and structurally to validate the assumption that they will perform comparably to their die cast originals.

To test this hypothesis further, subsequent engine testing was conducted by Gray et al. [59]. Their work demonstrated successful engine operation of the AM crankcase and cylinder head on two unique experimental setups using a dynamometer and propeller. Both configurations were instrumented to measure several parameters during operation, which then allowed for performance comparisons against the stock engine. Through these testing efforts, it was shown that although AM cylinder head and crankcase performed slightly worse that the cast original, the fully AM engine ran without failure or major damage for over 3.5 h during all testing performed. Additionally, it was determined that the AM engine's diminished performance most likely resulted from the choice to use a hypereutectic honing procedure rather than an iron liner. Therefore, these results help to prove that AM can be used to manufacture effective engine components.

6. Generalized metal LPBF process workflow summary

Although this work focused the metal LPBF additive manufacturing process through a specific example involving IC engine components, the overarching process can be used more widely with a variety of parts and applications. In general, going from an initial design to a final accepted part involves the following major steps:

1. *Initial design or reverse engineering*: First obtain or create a digital three-dimensional model of a component, then verify that it will fit within the build envelope of the machine, subsequently investigate that the part area consolidation relative to build area is not too high (≤20 % is recommended), and finally check that all thin features are ≥200 μm [19]. It is also within this step that material choice is made based on application requirements, this along with acceptable geometric tolerance then drives the decision for the manufacturing method used.
2. *Determine ideal build orientation and make model modifications*: Because metal AM is still relativity new when compared to traditional manufacturing methods, oftentimes initial designs are not optimized for AM, therefore model changes become necessary. Orientation and model modifications are grouped into one step here because of the direct influence they have on each other. Build orientation determines the areas that are considered “overhangs” which subsequently affects model modifications needed. Conversely, the material added for post-machining purposes can determine the best orientation for building. When considering build orientation, the goal should be to reduce the area of downskin surfaces that have ≤45° angle to the build plate [61], while also keeping the z cross-sectional area thickness consistent to reduce residual stresses. Additional model modifications generally include filleting sharp corners, filling horizontal holes, or adding material to surfaces that require machining. Machine stock is necessary when surface finish is important and/or tolerances are tight (usually ≤30 μm Ra [62] or ≤±0.25 to ±0.125 mm tolerance [19]), or a robust support is needed. In any case, it is important to keep design intent and end-use in mind while making these changes.

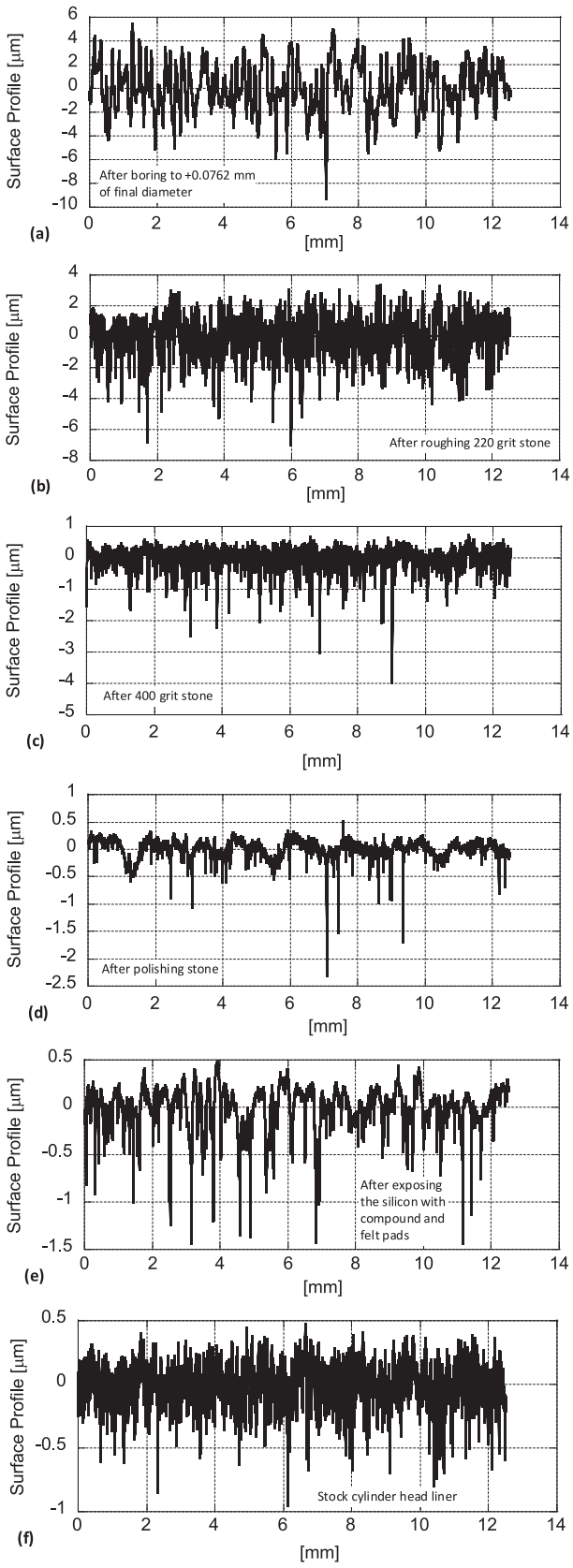

Fig. 12. Surface profile of AM cylinder head for each honing step compared to stock cylinder: (a) after boring, (b) after roughing 220 grit stone, (c) after 400 grit stone, (d) after polishing stone, (e) after compound and felt pads, and (f) stock cylinder head comparison.

3. *Build layout setup*: Build layout includes setting the orientation decided in the previous step and adding supports to the parts where needed. During this step, knowing cover gas flow and recoater directions are important for deciding the spacing of the components when there is more than one part [39–41]. Generally, staggering parts based on these two directions is important to prevent the potential for recoater tears, or fugitive upstream spatter, both of which can cause part defects. Additionally, angling the parts relative to the recoater helps ensure uniform powder distribution. It is also important to not overcrowd the plate with too many components as this can result in increased spatter defects and residual stress.
4. *Parameter choice and slicing*: The build file, which is what is loaded onto the machine, is created by slicing the entire build layout with the desired parameters. The parameters use for this step determine the slice/layer thickness, the vector path geometry (border(s) and hatch spacing), and laser power, speed, and focus assigned to every vector type (ex. downskin, border, hatch). Choosing validated parameters is critical to ensure part quality since these variables have the largest impact on the resulting roughness and porosity of the components [63].
5. *Post-processing*: Generally metal AM requires a bandsaw or wire Electrical Discharge Machining operation to remove the parts from the build plate if the supports have not been designed for hand breakoff. Other common post processing operations include heat treatment to obtain the desired mechanical properties and various machining operations.
6. *Inspection*: For a part in any industry to become an accepted production component, it almost always has to pass an inspection process. When it comes to inspection, intricate parts tend to require complex inspection techniques, and since metal AM lends itself to complexity, the inspection process tends to be its biggest hurdle in production qualification. The most common non-destructive inspection methods used, in order of complexity include: hand tools, gauges, coordinate measuring machine, structured light scanning, X-ray, and computed tomography [64,65]. Parts can also be inspected through functional testing if there are specific requirements that can be verified this way.

7. Conclusions

Using metal LPBF and several post processing methods, two major IC engine components (crankcase and cylinder head) were successfully produced with acceptable tolerances. These parts were first reverse engineered by taking measurements, modeling, and verifying the models through dimensional analysis. After choosing the materials and machines to be employed, these models were modified for AM construction while adding support structures. After manufacturing, the AM constructed components were checked for porosity and defects, before finally post machining. After machining, final CT scans showed that these parts should be comparable in performance to the cast originals. This was then proven through physical testing validation where the engine operated for 3.5 h without fail.

When considering the scale and cost of metal LPBF, it makes sense why the automotive industry has not yet adopted its use for consumer vehicles, outside of prototyping. However, when components are smaller, larger quantities can be manufactured at once. As a result, this gives AM a considerable advantage and provides potential to save on cost and lead times depending on the component. In addition, when part quantities are low, as is the case with military or luxury vehicles, there can be a cost advantage to choosing AM since it can absorb many of the upfront tooling costs. Nevertheless, another major disadvantage of metal AM comes from its additional post-processing requirements because of its rougher surface (closer to sand casting). Furthermore, any support material used generally requires a deburr process followed by some sort of filing or machining of the downskin surface. This could also become a post-processing advantage though, as machining aids can be printed

Fig. 13. Finished AM crankcase (top) and cylinder head (bottom).

directly on the part and later removed, which can reduce post-processing time and fixture needs. Overcoming many of these negatives, is metal AM's biggest advantage; its ability to achieve intricate geometric designs that can be optimized to reduce weight, combine assembly components, or enhance functionality.

While this work presented many challenges, post-processing of the AM components determined that they appear reasonably approximate to their corresponding cast versions (i.e., no major discrepancies). By proving AM can successfully produce operational engine components on a small scale, this technology demonstrator shows that there is opportunity for implementation of its use in larger military UAVs. Although AM has many advantages, a similar amount of machining will still be required due to the tight tolerances and surface finishes typically required for ICEs. Therefore, more optimization efforts are needed to provide significant enough fuel savings and range improvement to justify AM's use in this realm.

CRediT authorship contribution statement

Jamee Gray: Methodology, Validation, Formal analysis, Investigation, Writing – original draft, Visualization. **Christopher Depcik:** Investigation, Supervision, Visualization, Writing – review & editing. **Jennifer M. Sietins:** Investigation, Resources. **Andelle Kudzal:** Investigation. **Ryan Rogers:** Investigation, Validation. **Kyu Cho:** Conceptualization, Supervision, Project administration.

Declaration of competing interest

The authors report there are no competing interests to declare.

References

[1] Gray J, Depcik C. Review of additive manufacturing for internal combustion engine components. SAE IntJEngines 2020;13:617–32. https://doi.org/10.4271/03-13-05-0039.

[2] Brackett D, Ashcroft I, Hague R. Topology optimization for additive manufacturing. In: 2011 International Solid Freeform Fabrication Symposium, Austin, Texas; 2011. https://doi.org/10.26153/tsw/15300.

[3] Pagerit S, Sharer P, Rousseau A. Fuel economy sensitivity to vehicle mass for advanced vehicle powertrains, SAE Technical Paper 2006-01-0665. 2006. https://doi.org/10.4271/2006-01-0665.

[4] Casadei A, Broda R. Impact of vehicle weight reduction on fuel economy for various vehicle architectures, in, Ricardo. The Aluminum Association; 2007. https://www.drivealuminum.org/research-resources/impact-of-vehicle-weight-reduction-on-fuel-economy-for-various-vehicle-architectures/.

[5] Goh GD, Agarwala S, Goh GL, Dikshit V, Sing SL, Yeong WY. Additive manufacturing in unmanned aerial vehicles (UAVs): challenges and potential. AerospSciTechnol 2017;63:140–51. https://doi.org/10.1016/j.ast.2016.12.019.

[6] Belgiorno G, Boscolo A, Dileo G, Numidi F, Pesce FC, Vassallo A, Ianniello R, Beatrice C, Di Blasio G. Experimental study of additive-manufacturing-enabled innovative diesel combustion bowl features for achieving ultra-low emissions and high efficiency. SAE IntJAdvCurrPractMobil 2020;3:672–84. https://doi.org/10.4271/2020-37-0003.

[7] Belmonte MAReyes, Copeland CD, Hislop D, Hopkins G, Schmieder A, Bredda S, Akehurst S. Improving heat transfer and reducing mass in a gasoline piston using additive manufacturing, SAE Technical Paper 2015-01-0505. 2015. https://doi.org/10.4271/2015-01-0505.

[8] Laureijs RE, Roca JB, Narra SP, Montgomery C, Beuth JL, Fuchs ERH. Metal additive manufacturing: cost competitive beyond low volumes. J Manuf Sci Eng 2017;139. https://doi.org/10.1115/1.4035420.

[9] Khajavi SH, Partanen J, Holmström J. Additive manufacturing in the spare parts supply chain. ComputInd 2014;65:50–63. https://doi.org/10.1016/j.compind.2013.07.008.

[10] Haba SA, Oancea G. Digital manufacturing of air-cooled single-cylinder engine block. IntJAdvManufTechnol 2015;80:747–59. https://doi.org/10.1007/s00170-015-7038-x.

[11] C. Saito Seisakusho Ltd. Saito FG-11: 4-stroke gasoline single engine operating instructions. https://www.horizonhobby.com/on/demandware.static/Sites-horizon-us-Site/Sites-horizon-master/default/Manuals/SAIEG11-Manual.pdf; 2021.
[12] U.S. Army Corps of Engineers. MIL-HDBK-115A DOD handbook U.S. Army reverse engineering handbook (guidance and procedures). https://www.wbdg.org/ffc/army-coe/military-handbooks/hdbk-115a; 2006.
[13] MES Inc.. Alloy data: aluminum die casting alloys. https://www.mesinc.net/wp-content/uploads/2015/05/Die-Casting-Aluminum-Selection-Guide.pdf; 2021.
[14] Callister J, William D, Rethwisch DG. Materials science and engineering: an introduction. 10th ed. Wiley; 2018.
[15] Gray J. Feasibility of metal laser powder bed fusion for major internal combustion engine components. Department of Mechanical Engineering, University of Kansas; 2020. Master of Science.
[16] Kass MD, Noakes MW, Kaul B, Edwards D, Theiss T, Love L, Dehoff R, Thomas J. Experimental evaluation of a 4-cc glow-ignition single-cylinder two-stroke engine, SAE Technical Paper 2014-01-1673. 2004. https://doi.org/10.4271/2014-01-1673.
[17] Carley L. Cylinder Bore Surface Finishes. In: Engine Builder. Babcox; 2000. http://www.enginebuildermag.com/2000/09/cylinder-bore-surface-finishes/.
[18] Ford Motor Company. Engine design: cylinder block, heads, and gaskets (ED 207) in EEC-IV technical education. 1990.
[19] Bhavar V, Kattire P, Patil V, Khot S, Gujar K, Singh R. A review on powder bed fusion technology of metal additive manufacturing. In: Badiru AB, Valencia VV, Liu D, editors. Additive manufacturing handbook. CRC Press; 2017.
[20] Cao L, Li J, Hu J, Liu H, Wu Y, Zhou Q. Optimization of surface roughness and dimensional accuracy in LPBF additive manufacturing. OptLaser Technol 2021;142:107246. https://doi.org/10.1016/j.optlastec.2021.107246.
[21] Seifi M, Salem A, Beuth J, Harrysson O, Lewandowski JJ. Overview of materials qualification needs for metal additive manufacturing. JOM 2016;68:747–64. https://doi.org/10.1007/s11837-015-1810-0.
[22] Ladani L, Sadeghilaridjani M. Review of powder bed fusion additive manufacturing for metals. Metals 2021;11:1391. https://doi.org/10.3390/met11091391.
[23] Ladani L. Additive manufacturing of metals: materials, processes, tests, and standards. DEStech Publications, Incorporated; 2021.
[24] Hussein A, Hao L, Yan C, Everson R, Young P. Advanced lattice support structures for metal additive manufacturing. J Mater Process Technol 2013;213:1019–26. https://doi.org/10.1016/j.jmatprotec.2013.01.020.
[25] Weaver JS, Heigel JC, Lane BM. Laser spot size and scaling laws for laser beam additive manufacturing. JManufProcess 2022;73:26–39. https://doi.org/10.1016/j.jmapro.2021.10.053.
[26] Belay GY, Kinds Y, Goossens L, Gurung K, Bosmans N, Diltoer R, Eraly J, Vervaeke M, Thienpont H, Van Hooreweder B, Van Erps J. Dynamic optical beam shaping system to generate gaussian and top-hat laser beams of various sizes with circular and square footprint for additive manufacturing applications. Procedia CIRP 2022;111:75–80. https://doi.org/10.1016/j.procir.2022.08.134.
[27] Zhai W, Zhou W, Nai SML, Wei J. Characterization of nanoparticle mixed 316 L powder for additive manufacturing. JMaterSciTechnol 2020;47:162–8. https://doi.org/10.1016/j.jmst.2020.02.019.
[28] 3D Systems. Direct metal printers specifications sheet. 2018.
[29] Ceccanti F, Giorgetti A, Citti P. A support structure design strategy for laser powder bed fused parts. Procedia StructIntegrity 2019;24:667–79. https://doi.org/10.1016/j.prostr.2020.02.059.
[30] NTN Bearing Corporation of America. Bearing fits. https://ntnamericas.com/wp-content/uploads/2020/03/brgfits.pdf; 2021.
[31] Carley L. Align yourself. https://www.enginebuildermag.com/2003/10/align-yourself/; 2003.
[32] Neale MJ. Bearings: a tribiology handbook. 2nd ed. Society of Automotive Engineers; 1993.
[33] Carley L. Performance gaskets & surface finishes. https://www.enginebuildermag.com/2013/04/performance-gaskets-surface-finishes/; 2013.
[34] Engine Australia. Interference fit of valve guides in cylinder heads. https://www.engineaustralia.com.au/wp-content/uploads/2018/04/SB026.pdf; 2018.
[35] Society of Automotive Engineers International. Valve guide information report. SAE International; 2017. https://doi.org/10.4271/J1682_201712.
[36] Carver A. Getting a “Good Seat”: the growth in the valve seat insert market. https://www.enginebuildermag.com/1997/02/getting-a-good-seat-the-growth-in-the-valve-seat-insert-market/; 1997.
[37] Han Q, Gu H, Soe S, Setchi R, Lacan F, Hill J. Manufacturability of AlSi10Mg overhang structures fabricated by laser powder bed fusion. MaterDes 2018;160:1080–95. https://doi.org/10.1016/j.matdes.2018.10.043.
[38] International Organization for Standardization. Additive manufacturing — design — requirements, guidelines and recommendations. 2018.
[39] Anwar AB, Pham Q-C. Study of the spatter distribution on the powder bed during selective laser melting. Addit Manuf 2018;22:86–97. https://doi.org/10.1016/j.addma.2018.04.036.
[40] Liu Y, Yang Y, Mai S, Wang D, Song C. Investigation into spatter behavior during selective laser melting of AISI 316L stainless steel powder. MaterDes 2015;87:797–806. https://doi.org/10.1016/j.matdes.2015.08.086.
[41] Wang D, Ye G, Dou W, Zhang M, Yang Y, Mai S, Liu Y. Influence of spatter particles contamination on densification behavior and tensile properties of CoCrW manufactured by selective laser melting. OptLaser Technol 2020;121:105678. https://doi.org/10.1016/j.optlastec.2019.105678.
[42] Zaeh MF, Branner G. Investigations on residual stresses and deformations in selective laser melting. ProdEng 2010;4:35–45. https://doi.org/10.1007/s11740-009-0192-y.
[43] Esmaeilizadeh R, Ali U, Keshavarzkermani A, Mahmoodkhani Y, Marzbanrad E, Toyserkani E. On the effect of spatter particles distribution on the quality of Hastelloy X parts made by laser powder-bed fusion additive manufacturing. JManufProcess 2019;37:11–20. https://doi.org/10.1016/j.jmapro.2018.11.012.
[44] Schey JA. Introduction to manufacturing processes. Boston; Toronto: McGraw-Hill; 2000.
[45] Sietins JM. X-ray computed tomography quantitative analysis: an introductory software guide for DataViewer and CTAn. US Army Research Lab; 2018. Report Number: ARL-TN-0880.
[46] Mayer H, Papakyriacou M, Zettl B, Stanzl-Tschegg SE. Influence of porosity on the fatigue limit of die cast magnesium and aluminium alloys. IntJFatigue 2003;25:245–56. https://doi.org/10.1016/S0142-1123(02)00054-3.
[47] Major JF. Porosity control and fatigue behavior in A356-T61 aluminum alloy (97-94). In: Transactions of the American Foundry Society. 105; 1998. p. 901–6.
[48] Almaghariz ES, Conner BP, Lenner L, Gullapalli R, Manogharan GP, Lamoncha B, Fang M. Quantifying the role of part design complexity in using 3D sand printing for molds and cores. IntJMetalcast 2016;10:240–52. https://doi.org/10.1007/s40962-016-0027-5.
[49] Edwards P, O'Conner A, Ramulu M. Electron beam additive manufacturing of titanium components: properties and performance. J Manuf Sci Eng 2013;135. https://doi.org/10.1115/1.4025773.
[50] Hibbeler RC, Yap KB. Mechanics of materials. 2018.
[51] Akgun E, Zhang X, Lowe T, Zhang Y, Doré M. Fatigue of laser powder-bed fusion additive manufactured Ti-6Al-4V in presence of process-induced porosity defects. EngFractMech 2022;259:108140. https://doi.org/10.1016/j.engfracmech.2021.108140.
[52] Mian MJ, Razmi J, Ladani L. Defect analysis and fatigue strength prediction of As-built Ti6Al4V parts, produced using electron beam melting (EBM) AM technology. Materialia 2021;16:101041. https://doi.org/10.1016/j.mtla.2021.101041.
[53] A.S.M. International. C. Handbook, ASM handbookVol. 4; 1991.
[54] Levkulich NC, Semiatin SL, Gockel JE, Middendorf JR, DeWald AT, Klingbeil NW. The effect of process parameters on residual stress evolution and distortion in the laser powder bed fusion of Ti-6Al-4V. Addit Manuf 2019;28:475–84. https://doi.org/10.1016/j.addma.2019.05.015.
[55] I. Battelle Memorial. Metals, C. Ceramics Information, L. Air Force Materials, Titanium alloys handbook. Columbus, Ohio: Metals and Ceramics Information Center; 1972.
[56] Pepi M, Thiel J, Bryant N, McWilliams B, Kudzal A, Sietins JM. Towards replacement of failed parts on the battlefield via metal casting in 3D-printed desert sand molds. https://www.mfpt.org/wp-content/uploads/2019/10/Pepi_MFPT-2019-Manuscript_v2_FK.pdf; 2019.
[57] Meara T. New honing options for hypereutectic aluminum cylinder bores. Modern Machine Shop; 2008. https://www.mmsonline.com/articles/new-honing-options-for-hypereutectic-aluminum-cylinder-bores.
[58] Sunnen Products Co.. Precision honing supplies. 2021.
[59] Gray J, Srivatsa C, Mattson J, Depcik C. Propeller and dynamometer testing of an additive manufactured small internal combustion engine. SAE IntJEngines 2023;16(1). https://doi.org/10.4271/03-16-01-0005.
[60] Dolder B. Measuring tools, geometry, and surface finish, in. Production Engine Remanufacturers Association; 2017. https://www.pera.org/measuring-tools-for-geometry-and-surface-finish/https://www.pera.org/measuring-tools-for-geometry-and-surface-finish/.
[61] Obeidi MA. Metal additive manufacturing by laser-powder bed fusion: guidelines for process optimisation. ResultsEng 2022;15:100473. https://doi.org/10.1016/j.rineng.2022.100473.
[62] Snyder JC, Thole KA. Understanding laser powder bed fusion surface roughness. J Manuf Sci Eng 2020;142. https://doi.org/10.1115/1.4046504.
[63] Wang D, Liu Y, Yang Y, Xiao D. Theoretical and experimental study on surface roughness of 316L stainless steel metal parts obtained through selective laser melting. Rapid PrototypJ 2016;22:706–16. https://doi.org/10.1108/RPJ-06-2015-0078.
[64] Chauveau D. Review of NDT and process monitoring techniques usable to produce high-quality parts by welding or additive manufacturing. WeldWorld 2018;62:1097–118. https://doi.org/10.1007/s40194-018-0609-3.
[65] Barrenetxea L, Minguez R, Etxaniz O, Ortega N, Plaza S. In: Inspection of 3D printing and advanced manufacturing processes using hybrid 3D metrological technologies. Cham: Springer International Publishing; 2020. p. 153–65. https://doi.org/10.1007/978-3-030-41200-5_17.